Journal of Materials Chemistry A

Accepted Manuscript

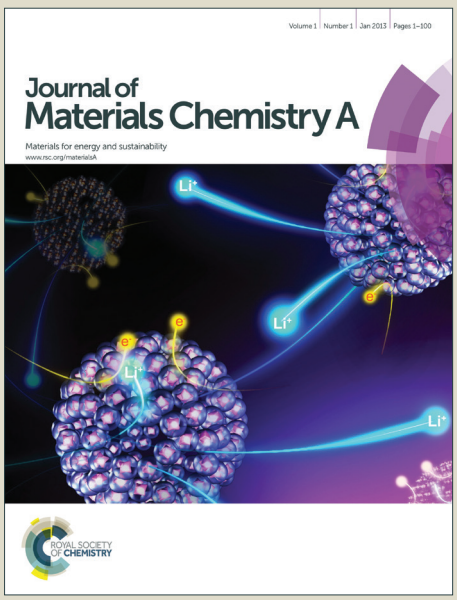

This is an *Accepted Manuscript*, which has been through the Royal Society of Chemistry peer review process and has been accepted for publication.

Accepted Manuscripts are published online shortly after acceptance, before technical editing, formatting and proof reading. Using this free service, authors can make their results available to the community, in citable form, before we publish the edited article. We will replace this *Accepted Manuscript* with the edited and formatted *Advance Article* as soon as it is available.

You can find more information about *Accepted Manuscripts* in the Information for Authors.

Please note that technical editing may introduce minor changes to the text and/or graphics, which may alter content. The journal's standard Terms & Conditions and the Ethical guidelines still apply. In no event shall the Royal Society of Chemistry be held responsible for any errors or omissions in this *Accepted Manuscript* or any consequences arising from the use of any information it contains.

ROYAL SOCIETY OF CHEMISTRY

www.rsc.org/materialsA

Journal Name

RSCPublishing

ARTICLE

Nanoflower-like Weak Crystallization Manganese Oxide for Efficient Removal of Low-concentration NO at Room Temperature

Jin Wang,[a] Jinzhen Zhu,[a] Xiaoxia Zhou,[a] Yanyan Du,[a] Weimin Huang,[a] Jianjun Liu,*[a] Wenqing Zhang[a], Jianlin Shi[a], and Hangrong Chen*[a]

Cite this: DOI: 10.1039/x0xx00000x

Received 00th January 2012,
Accepted 00th January 2012

DOI: 10.1039/x0xx00000x

www.rsc.org/

The efficient removal of low-concentration nitric oxide at room temperature in the semi-closed space is becoming a crucial but challenging issue in the context of increasingly serious air pollution. A novel nanoflower-like weak crystallization manganese oxide (WMO) has been synthesized *via* a facile and scalable strategy for low-concentration nitric oxide oxidation at room temperature. The prepared WMO shows the nanoflower-like morphology with abundant water molecules and Mn vacancies inside. Such WMO could easily adsorb NO and quickly convert it into NO_2 *via* catalytic oxidization. Herein, the weak crystallization structure and the presence of Mn vacancies are identified to be mainly responsible for the adsorption and catalytic oxidation of NO. More importantly, it shows much longer lifetime in a moist stream of simulated feed gas than that in a dry condition, which can be attributed to relative stability of catalyst with hydrated surfaces. Comparative DFT-calculations are performed to reveal catalytic effect of Mn-vacancy and hydrated surfaces in reducing the reaction barriers of rate-determining steps.

Introduction

There are more and more parking lots and road tunnels being constructed accompanying the expansion and development of big cities. However, the low ventilated efficiency of these semi-closed spaces tends to the accumulation of vehicle exhausts, causing the risk of health problem. For example, about several to tens of ppm nitrogen oxide (NO_x) (generally 90% nitric oxide and the rest is nitrogen dioxide) has been detected, owing to the incomplete removal and enrichment of NO_x,[1-3] which is much higher than the ambient air quality standard in China (less than 0.05 ppm NO_x, GB3095-2012). Thus, *in situ* removal of NO_x at room temperature from semi-closed spaces is in urgent demand. NO_x storage/reduction (NSR)[4, 5] and selective catalytic reduction (SCR)[6], which reduces high-concentration NO_x into N_2, are the most developed NO_x removal techniques. However, these two methods inevitably need high temperature, which are not suitable for NO_x removal at room temperature in semi-closed spaces. Hence, a new approach for de-NO_x at room temperature is of great demands. Very different from nitrogen dioxide (NO_2), which can be easily removed by alkali absorption, nitric oxide (NO) in ambient temperature and pressure is a kind of supercritical gas (Tc = 180 k), which is difficult to simply use physical adsorption removal.[7-9] When exposed to oxygen, NO will rapidly convert into reddish brown nitrogen dioxide at high enough amounts due to the low standard molar reaction enthalpy of NO_2 (−57.0 kJ·mol^{-1}, Eq. (1)). However, when the NO concentration drops to 10 ppm, such as under parking garages and road tunnels conditions, the NO molecules become much more stable due to greatly down-slowed oxidation at such low concentrations. According to the NO oxidation kinetics equation, the NO oxidation rate is inversely proportional to the square of the concentration of NO (Eq. (2)), therefore, one of the most important issues is to find a suitable catalyst that can effectively adsorb NO and accelerate its catalytic oxidation to NO_2, then absorbed by alkali to achieve the purpose of complete removal and purifying.

$$NO(g) + 1/2\ O_2(g) \rightarrow NO_2(g)$$
$$\Delta r H_m^{\ominus} = -57.0\ kJ{\bullet}mol^{-1} \quad (1)$$
$$r_{NO} = -k_1 P_{NO}^2 P_{O2} \quad (2)$$

Platinum/platinum-based catalysts[10-14] have been found to be especially active for nitric oxide oxidation and are widely used for mobile applications through fast SCR process. Nevertheless, they suffer from issues of such as weak thermal durability and high cost. Variously reported catalysts, such as Co_3O_4[15], Co-based catalysts[16, 17], MnO_x/TiO_2[18, 19], perovskite[20-22], Ru[23], activated carbon[24-26], zeolites[27-29] *etc.* have also been studied for NO oxidation under hundreds of ppm (the case for fuel exhaust gases) and manifested their highest NO conversion (less than 100%) around 300 °C. However, very low NO conversion

Journal of Materials Chemistry A Accepted Manuscript

efficiency has been found when they used in the oxidation of low-concentration NO with tens or lower ppm.[25] Therefore, it is still a great challenge to seek for a suitable catalyst in the catalytic process of low-concentration (e.g., 10 ppm) NO oxidation at room temperature, and few reports can be found till present. Recently, our group reported that many kinds of mesoporous Mn-based composite oxides could be used as outstanding heterogeneous catalysts for removal of low-concentration NO at room temperature.[30, 31] Nevertheless, such materials still have the drawbacks of short duration and weak water resistance, which limits the further practical application. Therefore, much interest and urgent demands are required for the development of low-cost, high water-resistant, and more durable NO oxidation catalysts.

Manganese oxides naturally occur in at least 30 different crystal structures[32], exhibiting different morphologies, and possess a variety of applications.[33-38] Therein, amorphous manganese oxide has been reported to have high catalytic activity for various reactions,[10, 39-44] which can be ascribed to the ease of lattice oxygen mobility and excess surface oxygen.[39] In spite of numerous studies on the catalytic performance of manganese oxide, reports on the exploration of manganese oxide as the high-efficiency catalyst for low-concentration NO removal at room temperature has not been found.

Herein, a novel week crystallization manganese oxide (WMO) with nanoflower morphology has been designed and synthesized *via* a facile redox-precipitation method for room temperature removal of low-concentration NO. NO removal activity measurements were conducted under both dry and 60% relative humidity inlet conditions. It was found that large numbers of manganese vacancies existed in WMO and the adsorbed water molecules on the Mn active sites, as well as week crystalline structure play a crucial role in determining the performance of catalyst. This prepared novel MO demonstrates a longer lifetime for low-concentration NO removal at room temperature, both in dry and moist stream of simulated feed gas. DFT-based first-principles calculations were firstly performed to reveal catalytic mechanism of different surface status. Their kinetic enhancement for NO catalytic oxidation and catalysis duration are understood based on the calculated potential energy profiles and thermodynamics.

Experimental

Synthesis details

WMO powder sample. WMO was synthesized by a facile redox-precipitation method.[13, 45] In brief, 0.732 g of $MnSO_4 \cdot H_2O$ was initially dissolved in 3 mL distilled water. Then, 0.485 g of $KMnO_4$ was dissolved in 8 mL distilled water and added to the above solution dropwise following by vigorous stirring. After adding 0.5 mL of nitric acid solution to the above solution and stirring for 12 hours under 40 °C. The product was filtered, washed several times with deionized water and dried at 80 °C. After 14 hours, week crystallization manganese oxide was obtained.

Monolithic catalyst. A honeycomb ceramic was immersed in Al_2O_3 slurry for 10 minutes and then dried in an oven, repeated three times and then calcined under 600 °C for 4 hours. The as-prepared WMO was dispersed in water, the Al_2O_3-coated honeycomb ceramic was immersed in the solution for 10 minutes and dried at 80 °C for 14 hours.

Characterization

XRD patterns were recorded on a Rigaku D/Max 2200PC diffractometer using Cu Kα radiation at 40 kV/40 mA, measured with a rate of 4°/min. The field emission scanning electron microscopy (SEM) analysis was performed on a JEOL JSM6700F electron microscope. Field emission transmission electron microscopy (TEM) analysis was conducted on a JEOL 200CX electron microscope operated at 200 KV. Nitrogen adsorption-desorption isotherms at 77 K were measured on a Micromeritics TriStar 3000 porosimeter. All samples were outgassed at 150 °C for 6 h under flowing nitrogen before measurements. The specific surface areas were calculated with the Brunauer-Emmet-Teller (BET) methods. Thermogravimetric/differential thermal analyzer mass spectrometry (TG-DTA-MS) measurements were performed using a Netzsch STA 449C apparatus with airflow of 20 mL/min and a heating rate of 10 K/min. The Fourier transform infrared (FTIR) spectra were performed on a Nicolet iS10 FTIR spectrometer with a resolution of 4 cm^{-1}. X-ray photoelectron spectroscopy (XPS) signals were collected on a Thermo Scientific ESCALAB 250 instrument using monochromated Al X-ray resource at 1486.6 eV operated at 15 kW. All the elemental binding energies were referenced to the C (1s) line situated at 285 eV. Potassium content were collected on an Agilent 710 Inductively Coupled Plasma Optical Emission Spectrometry (ICP-OES) by dissolved a certain amount of WMO in aqua regia.

NO removal activity measurements.

Simulated gas measurement. The catalytic properties of NO oxidation for samples were conducted in a quartz-tube plug flow reactor using 100 mg catalyst in a mixed gas of 10 ppm NO (similar to the level in the air of road tunnels and parking garages) and 21% O_2 balanced with N_2 at a flow rate of 200 $mL \cdot min^{-1}$ corresponding to a gas hourly space velocity of 40,000 h^{-1} under ambient condition. Then, the concentration of NO, NO_2 and NO_x in the inlet and outlet gas were online monitored by a NO_x analyzer (Thermo Fisher 42i-LS). The NO removal ratio was calculated as follows:

$$\text{NO removal ratio (\%)} = \frac{[NO]_{inlet} - [NO]_{outlet}}{[NO]_{inlet}} \times 100 \quad (3)$$

where $[NO]_{inlet}$ and $[NO]_{outlet}$ are the NO concentrations in the inlet and outlet gas, respectively. The inlet gas was humidified by passing through a bottle of deionized water and a relative humidity of 40% - 60% (changed with outer circumstance temperature) was achieved in the reactant gas.

Real engine exhausts measurement. The exhaust was produced by a diesel engine with going through an electrostatic precipitation equipment before measurement. The exhaust

Journal of Materials Chemistry A Accepted Manuscript

contains not only NO_x, but also CO, CO_2, HC and water vapor. The tested relative humidity was 69%.

Computational details

The first principle calculations were performed with the Vienna ab initio simulation package (VASP). The exchange-correlation energy has been calculated with the PBE functional. The structures have been relaxed until a maximum force of <0.02eV/Å and the energy convergence criterion is 10^{-6} eV. The electron-ion interactions were described by projector augmented wave (PAW) potential and the valence electrons were treated explicitly with a plane-wave basis set at a cutoff energy of 450 eV. As WMO possesses weak crystallinity and transition structure, will expose several active facets to an extent. Our calculations were performed on (211) surface of α-MnO_2, since (211) surface is more likely to absorb water than (2-2-1) surface and exhibits steps of the surface due to the reported results.[46] The models were calculated with a 4x5x1 k-points grid. A supercell with a vacuum space larger than 15 Å along z direction was used to simulate the surface. The +U correction term was not used in the present studies because the scheme correcting for the self-interaction of TM d-orbitals does not obviously improve molecular adsorption energies on the MnO_2 surfaces. Our test calculations using U = 4.5 eV [47] for Mn^{4+} indicates that NO adsorption energy on MnO_2 clean surface only has the energy difference of 0.01 eV compared with the corresponding calculation without +U correction.

For reducing the computational cost, our surface calculations in the present paper were performed by using 4-layer MnO_2. Test calculations for NO adsorbed on clean MnO_2 (211) surface show that adsorption energy using a 6-layer surface model with fixed 3 bottom layers presents almost equivalence to the 4-layer one. The NO adsorption energy on the 4-layer MnO_2 is 0.07 eV lower than that on the 6-layer MnO_2. Furthermore, the difference between two corresponding Mn−O bond lengths in the 4-layer and 6-layer structures is less than 0.06 Å. Therefore, the energy and structure changes almost are negligible due to the different layer models. The adsorption energies of NO and O_2 are calculated by the following equation:

$$E_{ads}(X) = E_{surf}(X) + E_{gas} - E_{surf+gas}(X) \quad (4)$$

where $E_{ads}(X)$ represents the adsorption energy, and E_{gas} is the energy of NO or O_2. $E_{surf}(X)$ and $E_{surf+gas}(X)$ are the energy of the surface without and with adsorbent, respectively.

Results and discussion

Characteristics of catalyst

The basic structural unit of all the manganese oxides corresponds to [MnO_6] octahedron. Different crystalline can be obtained through diverse packing manners of octahedra.[45, 48] The scanning electron microscopy (SEM) reveals that the prepared WMO consists of aggregated nanoparticles (Fig. 1a), which appears nanoflowers morphology observed by amplified image (Fig. 1b). Also, those nanoflowers are constituted by plate-like nanopetals with small number of randomly stacked octahedral sheets formed by edge-sharing [MnO_6] octahedra. The clearly detected lattice fringe shown in the high resolution transmission electron microscopy (HRTEM) image (Fig. 1c) and its corresponding selected area of electronic diffraction (SAED, inset of Fig. 1c) confirm the weak crystallinity of WMO. The XRD pattern of WMO (Fig. 2) compares well with previously reported manganese oxides.[45, 49, 50] WMO contains only two broad peaks appearing at *d*-spacing 2.4 Å (37°) and 1.4 Å (67°), corresponding to (211) and (112) indicating that O is structurally related to hexagonal symmetry birnessite since the resulting d-spacing quotient (1.71) is close to √3. Compared to the diffraction patterns of MnO_2, the absence of 7.18 Å (12.3°) and 3.6 Å (24.8°) reflection peaks, indicates MO is a kind of vernadite, which is a random-stacked birnessite, *i.e.*, there are a very small number of randomly stacked octahedral sheets per diffracting particle.[45] In addition, the coarse XRD pattern suggests the weak crystallinity of WMO. Moreover, the α-MnO_2 by increasing reaction temperature from 40 °C to 70 °C or higher (Fig. 2) could be obtained, accompanying with morphology change from nanoflower-like to rod-like (Fig. S1). The BET surface area of WMO shows as high as 346 m^2/g (N_2 adsorption–desorption isotherms see Supplementary Fig. S2), which is beneficial for the exposure of actives sites, and promoting the oxidation of NO at room temperature.

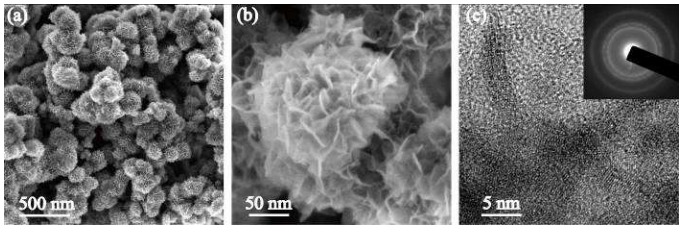

Fig. 1 SEM images (a), (b) and HRTEM image (c) of WMO (The inset is the corresponding selected area of electronic diffraction).

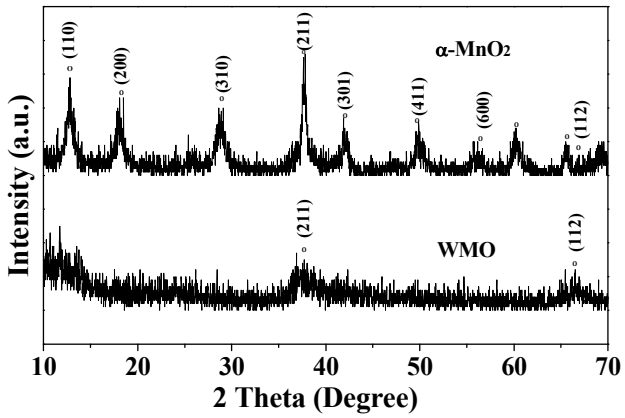

Fig. 2 XRD patterns of WMO and α-MnO_2.

XPS spectra were measured on the prepared WMO, and the references pure MnO_2, Mn_2O_3 and MnO for comparison to distinguish the different Mn valence states, and the binding

Journal of Materials Chemistry A Accepted Manuscript

energies are summarized in Supplementary Table S1 and Fig. S3a. Compared with the references pure MnO_2, Mn_2O_3 and MnO, the Mn 2p binding energy of the prepared WMO is very close to that of MnO_2, indicating that tetravalent Mn accounts for the vast majority. The calculated water content of the prepared WMO is around 14 wt% from the TG-DTA-MS curves (Table 1), since H_2O (18) signal could be detected during the test (see Supplementary Fig. S4). FT-IR data (see Supplementary Fig. S5a) were also collected to confirm that there were large amount of water molecules and/or hydroxyl groups within WMO. The peak at 1630 cm^{-1} is ascribed to the O–H bending vibration of water molecules adsorbed by the surface of WMO. The peaks between 1040 cm^{-1} and 1400 cm^{-1} are attributed to the bending stretching of H–O–H of the crystal water within the sample. According to the ICP results, the prepared sample has a lower potassium content (2.6%, Table 1) compared to δ-MnO_2 or "c-disordered" H^+-Birnessite.[45] The existence of potassium ions is indicative of negative structural charge, arising from the presence of Mn vacancies, where Mn atoms are absent in the octahedral sheets.[45] Thus, negative charges will be generated per vacant site, where hydrated interlayer cations can balance the negative charge, and hold the octahedral sheets together. The different O/Mn ratios obtained from XPS are summarized in Table 2. The distinctive deviation from stoichiometric ratio for the etched surface of the prepared WMO, *i.e.,* O/Mn equals to 2.21, confirms the presence of Mn vacancies. While, the much higher surface O/Mn ratio of 3.19 not only indicates the presence of Mn vacancies, but also the existence of large number of adsorbed oxygen species, which is also confirmed by the O 1s spectrum of XPS results in Fig. S2b. The missing of manganese atoms could induce the formation of oxygen dangling bonds, which may beneficial to the adsorption and catalytic oxidation of NO. Meanwhile, manganese atoms on the surface can also absorb water molecules to form H_2O–Mn structure. Therefore, it is believed that the calculated 14 wt% water content of the prepared WMO exists in both between the layers and the surface Mn sites of WMO *via* adsorption.

The removal performance of NO

Fig. 3 shows the results of low-concentration NO catalytic removal property of WMO at room temperature, by detecting the *in situ* time history of outlet gas concentration. The whole NO removal process can be divided into four steps. At first, no NO signals could be detected within the outlet gas, demonstrating NO could be completely adsorbed by WMO. Conversely, the NO_2 concentration is about 1 ppm, confirming that WMO can catalytic oxidize NO into NO_2 to some extent. The generated NO_2 outlet gradually declines to the minimum concentration of 0.3 ppm in the first hour, suggesting that the NO_2 product can be gradually adsorbed by WMO during the first stage of catalytic process. Next, the outlet NO_2 concentration increases with time going on while there's still no NO can be detected, indicating that WMO could adsorb NO and thoroughly convert it to NO_2 *via* catalytic oxidization. However, the capability of WMO for NO_2 adsorption gradually weakened owing to the cover of activity sites. Afterwards, NO could be detected from the outlet gas and its concentration gradually increases, accompanying with continuing increases of NO_2 concentration, indicating that the prepared WMO has lost the adsorptive activity for NO, but can still catalyze it into NO_2. Finally, NO_2 concentration decreases, accompanying with the concentration of NO gradually increases, indicating that WMO has gradually lost both the adsorptive capability for NO_2 and catalytic activity. The detailed results of NO removal ratio can be found in Fig. 3. In brief, this novel WMO possesses 100% NO removal capability under dry inlet condition and lasts for about 20 hours, which is 5 folds duration time of that reported before.[30] For comparison, the reference of well-crystallized α-MnO_2 shows no capability for NO removal (Fig. S6), suggesting that the weak crystallization of manganese oxide is one of the main reasons for the NO removal.

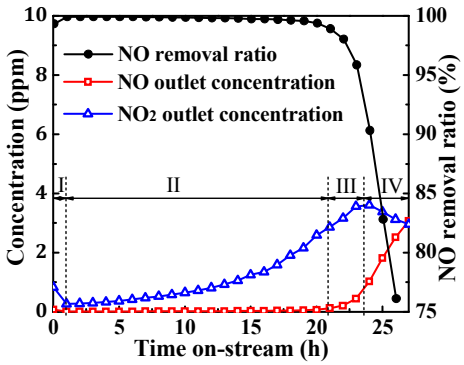

Fig. 3 Time course of outlet NO and NO_2 concentrations and NO removal ratios during NO removal test for WMO. Reaction conditions: [NO] = 10 ppm, [O_2] = 21%, balance = N_2, temperature = 25 °C, and GHSV = 40,000 h^{-1}.

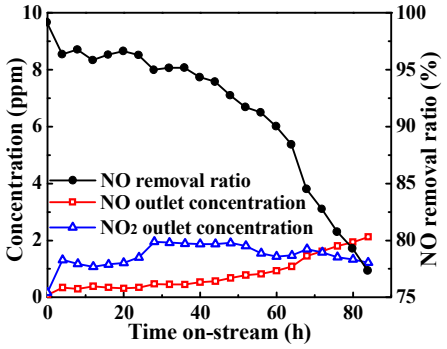

Fig. 4 Time course of outlet NO and NO_2 concentrations and NO removal ratios during NO removal test for WMO. Reaction conditions: [NO] = 10 ppm, [O_2] = 20%, balance = N_2, temperature = 25 °C, and GHSV = 40,000 h^{-1}, 60% relative humidity.

Furthermore, the water-resisting property of the prepared WMO was also tested with 60% relative humidity. Generally, water was found to be harmful in the NO removal process on Fe-Mn oxide catalyst.[30] Very interesting, this WMO shows much more excellent performance in the removal of NO under 60% relative humidity inlet condition (Fig. 4) than that in the

Journal of Materials Chemistry A Accepted Manuscript

dry inlet condition. Though it doesn't reach 100% of NO removal, it presents much longer duration of more than 70hrs for >80% NO removal ratio than that of only 25hrs in dry condition. However, during the whole NO removal test process, nitrite and nitrate are also observed according to FT-IR measurement, as shown in Fig. S5. The enhanced peak intensity at 1384 cm^{-1} compared to 1400 cm^{-1} can be attributed to the formation of nitrate species.[30, 51] Their gradual accumulations on catalytic surfaces could lead to gradual deactivation of active sites.

On the basis of these experimental results, a possible model has been proposed to explore the atomic-level insight into the fundamental catalytic mechanism. Since the prepared WMO has a weak crystallinity and high surface area with nanoflower-like morphology, it could possess large amount of structural defects and expose much more active facets, such as (211) surface, as shown in the XRD pattern (Fig. 2), to a certain extent. The previously fundamental studies have revealed[8, 46, 52, 53] that high-index surfaces exhibit much higher catalytic activity than low-index surfaces, since high-index surfaces have a higher density of unsaturated atomic steps, ledges, and kinks, which can serve as active sites for breaking chemical bonds. Therefore, the (211) surface was used as the active surface to catalyze $2NO + O_2 \rightarrow 2NO_2$. The DFT-based first-principles calculations were performed to obtain reaction paths of $2NO + O_2 \rightarrow 2NO_2$ on clean, Mn-vacancy, hydrated surfaces respectively, in order to reveal the influence of both Mn-vacancy and water on reaction mechanism and kinetics. The NEB method is used to locate the transition states connecting with two intermediates. The calculated reaction paths on three different surfaces are presented in Fig. 5a, b and c, respectively. Their corresponding reaction paths are listed in Fig. S7.

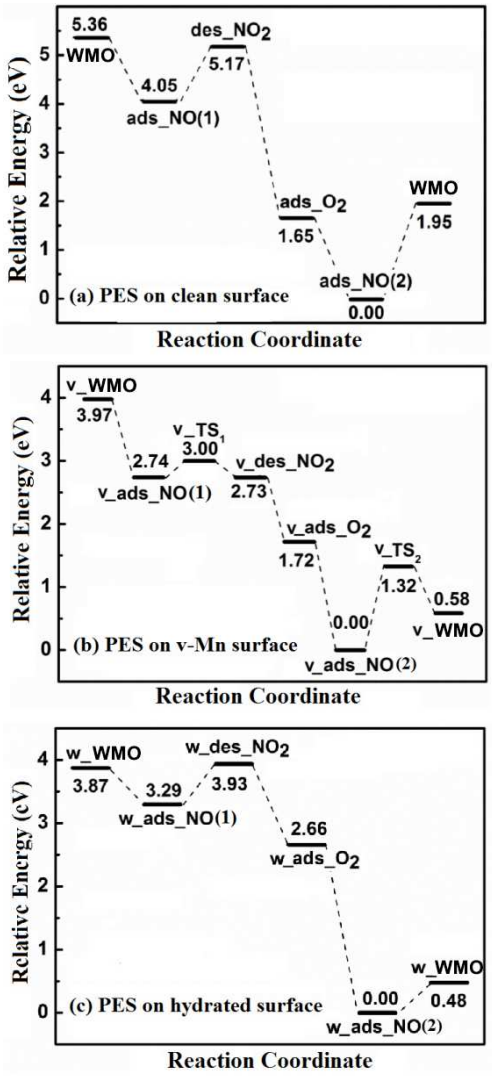

Fig. 5 DFT-calculated reaction paths of $2NO+O_2 \rightarrow 2NO_2$ on (a) clean MnO_2 (211), (b) Mn-vacancy surface, and (c) hydrated MnO_2 surface.

For the case of clean surface (Fig. S6A), NO is firstly adsorbed on four-coordinated Mn site by forming Mn–O bond. The adsorption energy is -1.31 eV (Fig. 5a) indicating that N–O bond can be strongly activated. Subsequently, the activated NO easily reacts with low-coordinated lattice oxygen (O_{lat}, Fig. S7A) to form NO_2. Thus it can generate an oxygen vacancy accompanying with NO_2 desorption. Afterwards, O_2 are easily adsorbed to form adsorbed oxygen (O_{ads}), which can be further activated on O-vacancy surface. Finally, the second NO_2 is desorbed followed by next NO adsorption. In terms of our calculated potential energy profiles (Fig. 5a-c), desorption of NO_2 requires surmounting higher energy barriers and are rate-determining in the catalytic processes. Therefore, it is very important to reduce reaction barriers of NO_2 desorption to enhance reaction kinetics. From XPS results of surface O 1s (see Supplementary Fig. S3b and Table 2), it can be found that before and after tests, the ratio of O_{lat} to O_{ads} decreases from 1.74 to 0.78, confirming that O_{lat} species were consumed during

Journal of Materials Chemistry A Accepted Manuscript

NO removal process. Further test was performed in a dry inlet condition but without using any oxygen within the inlet gas (see Supplementary Fig. S8), WMO also can last for about 2 hours of 100% NO removal, confirming the role of lattice oxygen cycle during the test.

In the case of the existence of Mn-vacancies (V''_{Mn}) in (211) surface (Fig. S7B), much more active O atoms with dangling bonds (O_{dan}) were formed around Mn vacancies. NO molecules were firstly adsorbed in the sites of O_{dan}, then the adsorbed NO (designated as NO_{ads}) can be activated to NO^+ (Eq. (5)) through electron transfer to the surface Mn^{4+} site (Eq. (6)). Meanwhile, O_{dan} was activated by an electron from V''_{Mn}, resulting in the formation of O^- (Eq. (7)), accompanying with V''_{Mn} turning into V'_{Mn} by losing an electron (Eq. (8)). Afterwards, the reaction between the activated NO^+ and O^- can quickly produce NO_2. V'_{Mn} can seize an electron from Mn^{3+} to form V''_{Mn} (Eq. (9)), and Mn^{3+} turns into Mn^{4+} (Eq. (10)) at the same time. As shown in Fig. 5b, the first and second desorption energies of NO_2 can greatly decrease from 1.12 and 1.95 eV (clean surface) to 0.26 and 1.32 eV (Mn-vacancy surface), indicating that NO_2 can desorb easily in Mn-vacancy surface, thus produces an oxygen vacancy (*i.e.,* an O_{dan} vacancy). Comparing with reaction mechanism on clean surface, it can be found that the presence of Mn vacancies can significantly reduce reaction barriers of NO_2 desorption, which is favourable to enhance reaction kinetics of NO conversion into NO_2.

$$NO - e \rightarrow NO^+ \quad (5)$$
$$Mn^{4+} + e \rightarrow Mn^{3+} \quad (6)$$
$$O + e \rightarrow O^- \quad (7)$$
$$V''_{Mn} - e \rightarrow V'_{Mn} \quad (8)$$
$$V'_{Mn} + e \rightarrow V''_{Mn} \quad (9)$$
$$Mn^{3+} - e \rightarrow Mn^{4+} \quad (10)$$

Furthermore, it is worth exploring the distinctive water-assisted mechanism for $2NO + O_2 \rightarrow 2NO_2$ in the presence of moisture. On the hydrated surface (Fig. S7C), OH group is adsorbed on the four-coordinated Mn site by forming Mn–O bond. Both Mn and OH are exposed as possible active sites to interact with NO molecule. Nevertheless, NO approaching into OH is relatively unstable according to the calculation, which leads to NO adsorbed on the neighboured Mn site. In addition, the calculation results indicate that the hydrated surface of MnO_2 can effectively reduce NO_2 desorption barrier to 0.64 and 0.48 eV in comparison with reaction path on the clean surface (1.12 and 1.95 eV), as shown in Fig. 5a and c. It means that NO_2 molecules can easily desorbed from the active sites, promoting NO adsorption on the refreshed surface O_{dan} sites. However, the active Mn sites occupied by OH may lead to the reduction of catalytic sites, which is consistent with the results in Fig. 4 (NO removal ratio cannot reach 100% with 60% relative humidity test condition).

In order to reveal the thermodynamic stability of different catalytic structures WMO, v_WMO, w_WMO, and v_w_WMO, we further calculated the formation energies of these structures, as shown in Table 3. Herein, the formation energy is defined as $\Delta E_f = E_{catalyst} - E_{Mn\text{-}bulk} - E_{O2} - E_{OH} = E_{catalyst} - E_{Mn\text{-}bulk} - E_{O2} - 1/2(1/2E_{O2}+E_{H2O})$, where the last term $(1/2(1/2E_{O2}+E_{H2O}))$ is included only in the hydrated surfaces. Based on Table 3, it can be found that the surfaces (w_WMO and v_w_WMO) with water-coverage have the larger stability in thermodynamics than dry ones (WMO and v_WMO). The calculated results could give a possible explanation for the longer water-assisted duration of catalysis. Humidity could keep the outlet NO_2 concentration balance and present much longer duration (it can last for more than 60 hrs at above 90% NO removal ratio) in a moist stream of simulated feed gas than that in the dry condition, which is much important for the practical application.

The NO removal capability of WMO under real engine exhaust condition was further measured by a monolithic catalyst, which was prepared by the as-synthesized WMO coated onto the honeycomb ceramic carrier, as shown in Fig. S9. The tested relative humidity was 69% and the results were summarized in Fig. 6. With the start of diesel engine, the NO concentration could reach highest value of about 7 ppm, while the NO outlet concentration was about 3 ppm at first and decreased as time went on. With the stable working status of engine, the released exhausts gradually decreased and finally achieved the complete removal of NO and lasted for the last during the whole test process, suggesting WMO could be used as a potential good catalyst in the actual application.

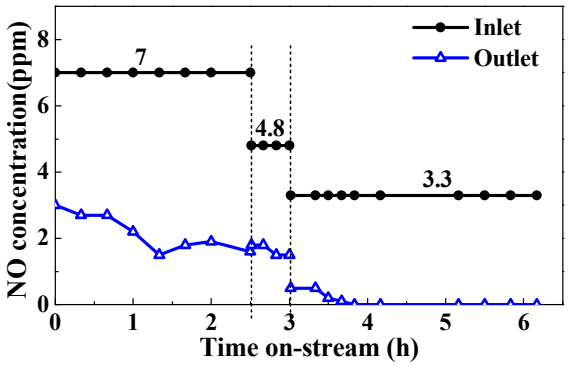

Fig. 6 Monolithic catalyst test. Inlet gas = diesel exhaust, velocity = 0.35 m•s^{-1}, temperature = 14 °C, relative humidity = 69%.

Table 1 Physicochemical properties of the prepared WMO.

BET Surface Area (m^2/g)	K+/Mn ratio (mol %)	Water content (%)
346	2.6	14

Table 2 XPS results of the O 1s and O/Mn ratio of WMO before and after NO removal test under dry inlet condition.

WMO	Fresh	After dry inlet test
O_{lat}/O_{ads}[a]	1.74	0.78
Surface O/Mn	3.19	3.28
Etched surface O/Mn	2.21	2.16

[a]O_{lat}: lattice oxygen, O_{ads}: adsorbed oxygen.

Journal of Materials Chemistry A Accepted Manuscript

Table 3 DFT-calculated formation energies (eV) of various catalytic structures including clean WMO, Mn-vacancy (v), hydrated (w) surfaces. The calculated values are based on one Mn atom.

	WMO	v_WMO	w_WMO	v_w_WMO
ΔE_f	-4.015	-4.066	-4.245	-4.193

Conclusions

In conclusion, a facile redox-precipitation method has been proposed to synthesize a novel week crystallization manganese oxide (WMO) with high surface area (>300 m^2/g), which can be used as an excellent adsorbent/catalyst for the removal of low-concentration NO at room temperature. The small amount of K ions indicates the presence of Mn vacancies and oxygen dangling bonds, which is great beneficial to the adsorption and catalytic oxidation of NO molecules. A detailed catalytic mechanism is proposed based on the results of XPS analysis and the reference NO removal test without any oxygen in the inlet gas. The first-principles calculations indicate that both water and Mn-vacancy on WMO surface significantly reduce the barriers of NO_2 desorption which is determined as the rate-determining step in $2NO + O_2 \rightarrow 2NO_2$ reaction. The calculated formation energies for the various catalytic structures suggest that the hydrated WMO surfaces are more stable than dry surfaces, which is the possible cause for longer duration of catalytic activity in a moist stream. However, these active Mn on hydrated surfaces may be occupied by OH^- so than interaction between NO/O_2 and Mn is hindered. Therefore, around 14 wt% water molecules existed in the prepared WMO calculated by TG-DTA-MS is considered to benefit the release of NO_2 and reducing the catalyst deactivation. More importantly, the prepared sample shows effective purification capability using a monolithic catalyst, indicating the potential application of such non-precious catalyst for the adsorption and catalytic oxidation of low-concentration nitric oxide at room temperature.

Acknowledgements

This research was sponsored by National Key Basic Research Program of China (2013CB933202), National 863 plans projects (2012AA062703), China National Funds for Distinguished Young Scientists (51225202) J. Liu acknowledges the One-Hundred-Talent Project and the Key Research Program (Grant No. KGZD-EW-T06) of the Chinese Academy of Science, the research grant (No.14DZ2261200) from Shanghai government.

Notes and references

[a]State Key Laboratory of High Performance Ceramics and Superfine Microstructure, Shanghai Institute of Ceramics, Chinese Academy of Sciences, 1295 Dingxi Road, Shanghai 200050, China. E-mail: hrchen@mail.sic.ac.cn. Fax: +86-21-52413122. Tel: +86-21-52415305. jliu@mail.sic.ac.cn. Tel: +86-21-52412801.

†

Electronic Supplementary Information (ESI) available: [details of any supplementary information available should be included here]. See DOI: 10.1039/b000000x/

1. M. Almeida-Silva, N. Canha, M. C. Freitas, H. M. Dung and I. Dionisio, *Applied Radiation and Isotopes*, 2011, **69**, 1586-1591.
2. G. L. Guerrini, *Constr Build Mater*, 2012, **27**, 165-175.
3. T. Maggos, J. G. Bartzis, M. Liakou and C. Gobin, *J Hazard Mater*, 2007, **146**, 668-673.
4. N. Takahashi, K. Yamazaki, H. Sobukawa and H. Shinjoh, *Applied Catalysis B: Environmental*, 2007, **70**, 198-204.
5. J. Klein, D. L. Wu, V. Tschamber, I. Fechete and F. Garin, *Applied Catalysis B: Environmental*, 2013, **132**, 527-534.
6. O. Monticelli, R. Loenders, P. A. Jacobs and J. A. Martens, *Applied Catalysis B: Environmental*, 1999, **21**, 215-220.
7. S. Hodjati, C. Petit, V. Pitchon and A. Kiennemann, *Applied Catalysis B: Environmental*, 2000, **27**, 117-126.
8. Z. R. Ismagilov and M. A. Kerzhentsev, *Catal Rev*, 1990, **32**, 51-103.
9. O. Monticelli, R. Loenders, P. A. Jacobs and J. A. Martens, *Applied Catalysis B: Environmental*, 1999, **21**, 215-220.
10. L. Olsson and E. Fridell, *Journal of Catalysis*, 2002, **210**, 340-353.
11. M. Koebel, G. Madia, F. Raimondi and A. Wokaun, *Journal of Catalysis*, 2002, **209**, 159-165.
12. E. Xue, K. Seshan and J. R. H. Ross, *Applied Catalysis B: Environmental*, 1996, **11**, 65-79.
13. J. Despres, M. Elsener, M. Koebel, O. Krocher, B. Schnyder and A. Wokaun, *Applied Catalysis B: Environmental*, 2004, **50**, 73-82.
14. N. Rankovic, A. Nicolle and P. Da Costa, *J Phys Chem C*, 2010, **114**, 7102-7111.
15. M. F. Irfan, J. H. Goo and S. D. Kim, *Applied Catalysis B: Environmental*, 2008, **78**, 267-274.
16. M. M. Yung, E. M. Holmgreen and U. S. Ozkan, *Journal of Catalysis*, 2007, **247**, 356-367.
17. H. Q. Wang, J. Wang, Z. B. Wu and Y. Liu, *Catal Lett*, 2010, **134**, 295-302.
18. Z. B. Wu, N. A. Tang, L. Xiao, Y. Liu and H. C. Wang, *Journal of colloid and interface science*, 2010, **352**, 143-148.
19. N. Tang, Y. Liu, H. Q. Wang and Z. B. Wu, *J Phys Chem C*, 2011, **115**, 8214-8220.
20. Y. Wen, C. Zhang, H. He, Y. Yu and Y. Teraoka, *Catal Today*, 2007, **126**, 400-405.
21. C. H. Kim, G. Qi, K. Dahlberg and W. Li, *Science*, 2010, **327**, 1624-1627.
22. S. O. Choi, M. Penninger, C. H. Kim, W. F. Schneider and L. T. Thompson, *ACS Catalysis*, 2013, **3**, 2719-2728.
23. L. D. Li, L. L. Qu, J. Cheng, J. J. Li and Z. P. Hao, *Applied Catalysis B: Environmental*, 2009, **88**, 224-231.
24. S. Adapa, V. Gaur and N. Verma, *Chem Eng J*, 2006, **116**, 25-37.
25. I. Mochida, Y. Kawabuchi, S. Kawano, Y. Matsumura and M. Yoshikawa, *Fuel*, 1997, **76**, 543-548.
26. P. Nikolov, M. Khristova and D. Mehandjiev, *Colloid Surface A*, 2007, **295**, 239-245.
27. H. Y. Liu, Z. K. Zhang, Y. Y. Xu, Y. F. Chen and X. Li, *Chinese J Catal*, 2010, **31**, 1233-1241.

Journal of Materials Chemistry A Accepted Manuscript

28. M. Iwamoto, A. M. Hernandez and T. Zengyo, *Chemical communications*, 1997, 37-38.
29. J. Shi, *Chemical reviews*, 2013, **113**, 2139-2181.
30. Z. Shu, Y. Chen, W. M. Huang, X. Z. Cui, L. X. Zhang, H. R. Chen, G. B. Zhang, X. Q. Fan, Y. X. Wang, G. J. Tao, D. N. He and J. L. Shi, *Applied Catalysis B: Environmental*, 2013, **140**, 42-50.
31. Z. Shu, W. M. Huang, Z. L. Hua, L. X. Zhang, X. Z. Cui, Y. Chen, H. R. Chen, C. Y. Wei, Y. X. Wang, X. Q. Fan, H. L. Yao, D. N. He and J. L. Shi, *J Mater Chem A*, 2013, **1**, 10218-10227.
32. J. E. Post, *Proceedings of the National Academy of Sciences of the United States of America*, 1999, **96**, 3447-3454.
33. H. Wang, G. Zhao and M. Pumera, *Journal of the American Chemical Society*, 2014, **136**, 2719-2722.
34. B. A. Pinaud, Z. B. Chen, D. N. Abram and T. F. Jaramillo, *J Phys Chem C*, 2011, **115**, 11830-11838.
35. X. Wang and Y. Li, *Journal of the American Chemical Society*, 2002, **124**, 2880-2881.
36. R. S. Kalubarme, M. S. Cho, K. S. Yun, T. S. Kim and C. J. Park, *Nanotechnology*, 2011, **22**, 395402.
37. S. K. Meher and G. R. Rao, *Journal of Power Sources*, 2012, **215**, 317-328.
38. B. Hu, S. Frueh, H. F. Garces, L. Zhang, M. Aindow, C. Brooks, E. Kreidler and S. L. Suib, *Applied Catalysis B: Environmental*, 2013, **132-133**, 54-61.
39. H. Cao and S. L. Suib, *Journal of the American Chemical Society*, 1994, **116**, 5334-5342.
40. S. R. Segal, S. L. Suib, X. Tang and S. Satyapal, *Chemistry of Materials*, 1999, **11**, 1687-1695.
41. H. C. Genuino, E. C. Njagi, E. M. Benbow, G. E. Hoag, J. B. Collins and S. L. Suib, *Journal of Photochemistry and Photobiology A: Chemistry*, 2011, **217**, 284-292.
42. J. C. Lin, J. Chen, S. L. Suib, M. B. Cutlip and J. D. Freihaut, *Journal of Catalysis*, 1996, **161**, 659-666.
43. C.-H. Chen, E. C. Njagi, S.-P. Sun, H. Genuino, B. Hu and S. L. Suib, *Chemistry of Materials*, 2010, **22**, 3313-3315.
44. J. Yang and J. J. Xu, *Electrochemistry Communications*, 2003, **5**, 306-311.
45. M. Villalobos, B. Toner, J. Bargar and G. Sposito, *Geochimica et Cosmochimica Acta*, 2003, **67**, 2649-2662.
46. L. Li, Z. D. Wei, S. G. Chen, X. Q. Qi, W. Ding, M. R. Xia, R. Li, K. Xiong, Z. H. Deng and Y. Y. Gao, *Chemical Physics Letters*, 2012, **539**, 89-93.
47. D. A. Tompsett, S. C. Parker, P. G. Bruce and M. S. Islam, *Chemistry of Materials*, 2013, **25**, 536-541.
48. D. M. Robinson, Y. B. Go, M. Mui, G. Gardner, Z. Zhang, D. Mastrogiovanni, E. Garfunkel, J. Li, M. Greenblatt and G. C. Dismukes, *J Am Chem Soc*, 2013, **135**, 3494-3501.
49. E. C. Njagi, C.-H. Chen, H. Genuino, H. Galindo, H. Huang and S. L. Suib, *Applied Catalysis B: Environmental*, 2010, **99**, 103-110.
50. S. Grangeon, B. Lanson, N. Miyata, Y. Tani and A. Manceau, *American Mineralogist*, 2010, **95**, 1608-1616.
51. H. Y. Huang and R. T. Yang, *Langmuir*, 2001, **17**, 4997-5003.
52. M. Behrens, F. Studt, I. Kasatkin, S. Kuhl, M. Havecker, F. Abild-Pedersen, S. Zander, F. Girgsdies, P. Kurr, B. L. Kniep, M. Tovar, R. W. Fischer, J. K. Norskov and R. Schlogl, *Science*, 2012, **336**, 893-897.
53. J. K. Norskov, T. Bligaard, B. Hvolbaek, F. Abild-Pedersen, I. Chorkendorff and C. H. Christensen, *Chemical Society reviews*, 2008, **37**, 2163-2171.

Journal of Materials Chemistry A Accepted Manuscript